ORIGINAL ARTICLE

Neuropathology and
Applied Neurobiology
JOURNAL OF THE BRITISH NEUROPATHOLOGICAL SOCIETY

WILEY

Differentiating idiopathic inflammatory myopathies by automated morphometric analysis of MHC-1, MHC-2 and ICAM-1 in muscle tissue

Anna Nishimura[1] | Christopher Nelke[2] | Melanie Huber[3] |
Alexander Mensch[4] | Angela Roth[1] | Christoph Oberwittler[5] |
Björn Zimmerlein[6] | Heidrun H. Krämer[7,8] | Eva Neuen-Jacob[9] |
Werner Stenzel[10] | Ulf Müller-Ladner[3] | Tobias Ruck[2] | Anne Schänzer[1,8]

[1]Institute of Neuropathology, Justus-Liebig University Giessen, Germany

[2]Department of Neurology, Medical Faculty and University Hospital Düsseldorf, Heinrich-Heine-University, Düsseldorf, Germany

[3]Department of Rheumatology and Clinical Immunology, Campus Kerckhoff, Justus-Liebig-University, Giessen, Germany

[4]Department of Neurology, University Medicine Halle, Halle (Saale), Germany

[5]Department of Neurology, St. Vincenz Hospital, Limburg, Germany

[6]Department of Neurology, Hospital Nordwest, Frankfurt, Germany

[7]Department of Neurology, Justus-Liebig-University, Giessen, Germany

[8]Translational Neuroscience Network Giessen (TNNG), Justus Liebig University Giessen, Giessen, Germany

[9]Institute of Neuropathology, Heinrich-Heine-University, Düsseldorf, Germany

[10]Department of Neuropathology, Charité - Universitätsmedizin Berlin, corporate member of Freie Universität Berlin and Humboldt-Universität zu Berlin, Berlin, Germany

Correspondence
Anne Schänzer, Institute of Neuropathology, Justus Liebig University Giessen, Germany.
Email: anne.schaenzer@patho.med.uni-giessen.de

Abstract

Aims: Diagnosis of idiopathic inflammatory myopathies (IIM) is based on morphological characteristics and the evaluation of disease-related proteins. However, although broadly applied, substantial bias is imposed by the respective methods, observers and individual staining approaches. We aimed to quantify the protein levels of major histocompatibility complex (MHC)-1, (MHC)-2 and intercellular adhesion molecule (ICAM)-1 using an automated morphometric method to mitigate bias.

Methods: Double immunofluorescence staining was performed on whole muscle sections to study differences in protein expression in myofibre and endomysial vessels. We analysed all IIM subtypes including dermatomyositis (DM), anti-synthetase syndrome (ASyS), inclusion body myositis (IBM), immune-mediated-necrotising myopathy (IMNM), dysferlinopathy (DYSF), SARS-CoV-2 infection and vaccination-associated myopathy. Biopsies with neurogenic atrophy (NA) and normal morphology served as controls. Bulk RNA-Sequencing (RNA-Seq) was performed on a subset of samples.

Results: Our study highlights the significance of MHC-1, MHC-2 and ICAM-1 in diagnosing IIM subtypes and reveals distinct immunological profiles. RNASeq confirmed the precision of our method and identified specific gene pathways in the disease subtypes. Notably, ASyS, DM and SARS-CoV-2-associated myopathy showed increased ICAM-1 expression in the endomysial capillaries, indicating ICAM-1-associated vascular activation in these conditions. In addition, ICAM-1 showed high discrimination between different subgroups with high sensitivity and specificity.

Conclusions: Automated morphometric analysis provides precise quantitative data on immune-associated proteins that can be integrated into our pathophysiological understanding of IIM. Further, ICAM-1 holds diagnostic value for the detection of IIM pathology.

INTRODUCTION

Idiopathic inflammatory myopathies (IIM) are classified according to the current integrated classification based on clinical, serological and morphological findings. These include dermatomyositis (DM), immune-mediated necrotising myopathy (IMNM), anti-synthetase syndrome (ASyS) and inclusion body myositis (IBM) [1–3]. Other myopathies, including hereditary disorders, may mimic IIM [4–6]. In addition, myopathy with inflammatory features associated with SARS-CoV-2 infection has been reported in patients with severe COVID-19 [7, 8]. These factors make the accurate diagnosis of IIM more challenging. However, a better understanding of the immune signature and a precise diagnosis are required to determine the optimal treatment approach for individual patients.

At the pathophysiological level, major histocompatibility complex (MHC) classes I and II play major roles in the adaptive immune system and are important for antigen presentation and recognition [9]. MHC-1 is an established marker for morphological IIM diagnosis, showing high sensitivity but low specificity [10, 11]. A recent study analysed MHC-1 and MHC-2 in a larger cohort of skeletal muscle biopsies from patients with IIM and reported high specificity for MHC-2 expression in patients diagnosed with IBM and ASyS [9, 12–15]. Protein expression was analysed in the DAB-stained sections using the scores determined by the observer, but precise protein quantification was not performed. Additionally, vascular pathology is poorly captured by MHC expression analysis.

Intercellular adhesion molecule 1 (ICAM-1) is a transmembrane protein essential for immune synapse formation, endothelial activation and leukocyte migration [16–18]. Furthermore, it is necessary as a co-stimulatory ligand for T-cell activation [19]. In dermatomyositis and mixed connective tissue increased vascular ICAM-1 expression indicates vascular involvement [9, 20, 21]. In previous studies, the results of protein expression in myositis varied significantly, making interpretation difficult. In addition, a quantitative approach is currently lacking [9, 22, 23]. Notably, ICAM-1 expression has not yet been analysed in recognition within the context of the current IIM classification and may be suited to depict vascular inflammation as well as myofibre pathology.

This study aimed to establish an automated, objective method to quantify protein expression in muscle fibres and endomysial vessels. We included muscle biopsies from patients with IIM subtypes and compared them with those from myopathies with an inflammatory component, neurogenic atrophy (NA) and non-diseased controls (NDC). This analysis aims to improve our understanding of the immunological signatures of IIMs and identify potential diagnostic markers.

> ## Key Points
>
> - Quantification of immune-associated proteins, such as MHC-1, MHC-2, and ICAM-1, at the protein and gene levels and identification of specific gene pathways can be integrated into our pathophysiological understanding of myositis and improve the diagnostic workflow.
> - ICAM-1 expression at the protein and gene levels provides distinct immune signatures in the various subgroups of myositis.
> - The vascular pathology observed in ASyS, DM, and myopathy related to SARS-CoV-2 infection may be related to ICAM-1-mediated endothelial activation.
> - With our data, we introduce ICAM-1 as a new diagnostic marker for the morphological classification of myositis.

METHODS

Patients

The patients were recruited from three German neuromuscular centres. Biopsies were obtained from all participants prior to our study for diagnostic reasons. The inclusion criterion was a diagnosis of IIM according to the current integrative classification [1, 24]. Informed Consent was obtained. Clinical and serological characteristics including myositis-specific antibodies (MSA), were retrospectively analysed. Additionally, skeletal muscle samples from patients with dysferlinopathy (DYSF), myopathy due to SARS-CoV-2 infection or SARS-CoV-2 vaccine-associated non-specific myositis (COVID-19) and NA, as well as NDCs, were included. NDCs were chosen according to clinical examination, including laboratory parameters, electrophysiological analysis and the absence of major pathology in muscle biopsy samples.

Skeletal muscle morphology

Skeletal muscle biopsies were processed according to standard routine procedures [25]. All biopsies were re-evaluated according to the current IIM classification [1, 2, 26, 27]. The degree of pathology severity, including inflammatory infiltration, muscle fibres alteration regeneration, degeneration, necrosis, internal nuclei, connective tissue variations and vascular features, was estimated on H&E-stained sections using a modified consensus ranking scale (VAS = Visual Analogue Score), as described previously [28, 29]. The pathology was

rated from normal (0) to severe (10). In addition, perifascicular atrophy (PFA), punched-out vacuoles (POV), regeneration, necrosis, oedema and inflammation were assessed using a score ranging from 0 to 3 in all specimens.

Immunofluorescence and immunohistochemical studies

Double immunofluorescence staining was performed for all skeletal muscle biopsies. Ten micrometers of thick frozen sections were fixed with cold 100% acetone for 10 min, washed, and then blocked with 10% goat serum (ab7481, Abcam) for 30 min at room temperature (RT). Primary antibodies were diluted with antibody diluent (S3022, DAKO), applied to the sections and incubated overnight at 4°C. The next day, secondary antibodies were applied after further washing steps and incubated for 2 h at RT, then washed and mounted using DAPI-aqueous (ab104139, Abcam). The following primary antibodies were used: MHC class I (ab134189, 1:200, Abcam), MHC class II (ab170867, 1:200, Abcam), ICAM-1 (ab109361, 1:25, Abcam), CD31 (Clone JC70A, 1:25, DAKO), spectrin (NCL-SPEC2, 1:200, NovoCastra) and desmin (Clone JC70A, 1:200, DAKO). Secondary antibodies: Goat anti-rabbit Alexa Fluor®568 and goat anti-mouse Alexa Fluor®488 (Abcam, 1:200–1:400). Immunohistochemistry with antibodies against ICAM-1 (ab109361, 1:100, Abcam) and CD45 (1:500, LCA antibody, DAKO) was performed using a benchmark automatic staining platform (Ventana, Heidelberg, Germany), visualised with Ultra View DAB Detection Kit v1.02.0018, Ventana Medical Systems. See detailed antibody information in Supplemental Table 1.

Automated morphometric analysis of protein expression on myofibre and endomysial vessels

Immunofluorescent sections were digitised using a Zeiss Axio Scan.Z1 slide scanner and the ZEN software. Scan settings included z-stacks (3 μm) for MHC-1/spectrin and MHC-2/spectrin staining and stitching configuration (offline stitching). The images were converted from czi files (Carl Zeiss format) to TIFF files using QuPath software to facilitate the analysis and to reduce file size. The thresholds for each channel (568 and 488) were set manually and used equally for every specimen. Each section's ROI (region of interest) was set manually. The entire section was analysed. Connective tissue and staining artefacts were manually excluded. Figure 1A shows a representative whole-section image of a DM with MHC-1/Spectrin staining. The Manders overlap coefficient (MOC) was used to estimate the degree of co-localisation of proteins (MHC-1, MHC-2 and ICAM-1) on muscle fibres (identified by either spectrin or desmin) using Fiji software and the plugin BIOP JACoP. A MOC of "0" indicates no co-localisation of the green and red channels and a MOC of "1" represents a complete co-localisation of both channels [30, 31] (Figure 1B).

To evaluate the intensity of ICAM-1 expression in endomysial vessels, the mean grey values (MGV) of areas that expressed both

ICAM-1 and CD31 were assessed using Fiji software. For this, an ROI was created for each channel and their intersection was used to create another ROI, which represented the area expressing both ICAM-1 and CD31 (Figure 1C). To determine the threshold, the Otsu method was used [32]. The observer was blinded to the specimens.

RNA library preparation and NovaSeq sequencing

RNA Sequencing was performed on 25 skeletal muscle samples stored in liquid nitrogen before use. Total RNA was extracted from tissue samples using the Qiagen RNeasy Mini Kit following the manufacturer's instructions (Qiagen, Hilden, Germany). RNA samples were quantified using a Qubit 4.0 Fluorometer (Life Technologies, Carlsbad, CA, USA), and RNA integrity was checked with an RNA Kit on the Agilent 5300 Fragment Analyser (Agilent Technologies, Palo Alto, CA, USA). RNA sequencing libraries were prepared using the NEBNext Ultra II RNA Library Prep Kit for Illumina according to the manufacturer's instructions (NEB, Ipswich, MA, USA). Briefly, mRNAs were first enriched with oligo (dT) beads. The enriched mRNAs were fragmented according to the manufacturer's instructions. First and second-strand cDNAs were subsequently synthesised. The cDNA fragments were end-repaired and adenylated at 3′ ends, and universal adapters were ligated to the cDNA fragments, followed by index addition and library enrichment by limited-cycle PCR. The sequencing libraries were validated using an NGS Kit on the Agilent 5300 Fragment Analyser (Agilent Technologies, Palo Alto, CA, USA), and quantified using a Qubit 4.0 Fluorometer (Invitrogen, Carlsbad, CA, USA). The sequencing libraries were multiplexed and loaded onto the flow cell on an Illumina NovaSeq 6000 instrument, according to the manufacturer's instructions. The samples were sequenced using a 2×150 Pair-End (PE) configuration v1.5. Image analysis and base calling were conducted on a NovaSeq instrument using the NovaSeq Control Software v1.7 on the NovaSeq instrument. The raw sequence data (.bcl files) generated by the Illumina NovaSeq were converted into fastq files and de-multiplexed using the Illumina bcl2fastq programme version 2.20. One mismatch was allowed for the index sequence identification.

Statistical analysis

Statistical analyses of the MOC, MGV and VAS scores in the muscle biopsy cohorts as well as the correlation of protein expression with clinical parameters were performed using GraphPad Prism 10. The nonparametric Mann–Whitney U test was used to determine differences between two individual subgroups, and the Kruskal–Wallis test was used for multiple comparisons including the uncorrected Dunn's test. Boxplots are shown as standard Tukey boxplots representing medians and the first and third quartiles. The Spearman's rank correlation coefficient was used to examine the correlation between protein expression and clinical parameters. Receiver operating characteristics (ROC) curves and the area under the ROC curves (AUC) were
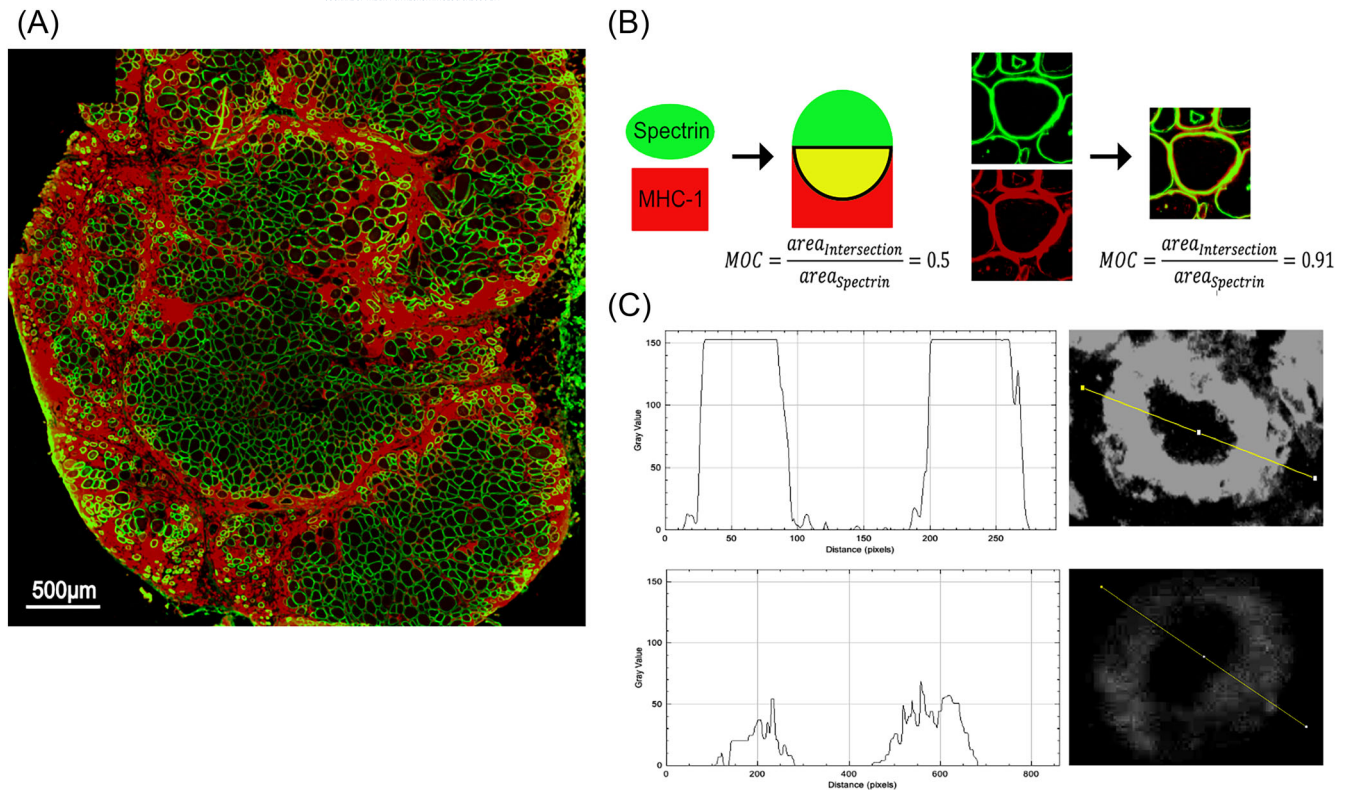
FIGURE 1 Method for automated quantification of protein expression: digitised whole sections with double immunofluorescence staining were used for automated morphometric analysis of protein quantification. A representative image of a case with DM stained with MHC-1 and spectrin (A). Co-expression of proteins on muscle fibres was estimated by the Manders overlap coefficient (MOC). MOC of "0" indicates no co-localisation of green and red channels. MOC of "1" represents a complete co-localisation of both channels (B). Co-expression of proteins on endomysial vessels was estimated by the mean grey value (MGV) (C).

calculated using GraphPad Prism 10. Sensitivity and specificity were determined using Youden's statistic [33]. Figures were created using Affinity Designer 2. p values are indicated as ≤0.05, ≤0.01 and ***≤0.001.

Bioinformatic analysis

To compare the protein levels between the subgroups, the mean values of the individual proteins in each subgroup were visualised using a heatmap with GraphPad Prism 9 software. Different colours indicate different protein levels. The results were normalised beforehand. For gene expression values, counts were generated using the R package Salmon. For differential expression testing, we used DESeq2 to generate a count data matrix for all samples. A principal component analysis (PCA) was performed for dimensional reduction. Each patient was treated as a single data point. The data were scaled and centred.

To analyse enriched pathways, we performed an Overrepresentation Analysis (ORA) of the Gene Ontology Biological Process (GO BP) database [34]. Differentially expressed genes (DEGs) were calculated for each entity using a two-sided gene pathway Student's t-test adjusted for multiple testing using the False Discovery Rate (FDR) set at 0.05. Each DEG list was calculated by comparing the corresponding entities with those of the controls. The DEG list was entered into WebGestalt (https://www.webgestalt.org/) using the GO BP database and standard settings.

RESULTS

Patients

Skeletal muscle biopsies of 59 patients (average age at biopsy 52 years; range 17–81 years; 59% female) were analysed in this study. Thirty-three patients were diagnosed with IIM, including DM (n = 9), IMNM (n = 7), ASyS (n = 6) and IBM (n = 11). The diagnosis was confirmed by clinical, morphological and serological findings. Six patients were genetically confirmed to have DYSF. Five patients presented with myopathy post-infection with SARS-CoV-2, and two patients with myopathy post-SARS-CoV-2 vaccination. NA (n = 5) and NDC (n = 8) served as controls (Figure 2A). The majority (81%) of the biopsies were obtained from the proximal part of the lower limb. However, 19% were taken from the proximal part of the upper limb. Twelve biopsies of IIM (36%) were obtained before the start of immune modulating therapy.I n 21 patients (64%) biopsies were obtained shortly after the onset of therapy (maximum 4 weeks). The detailed
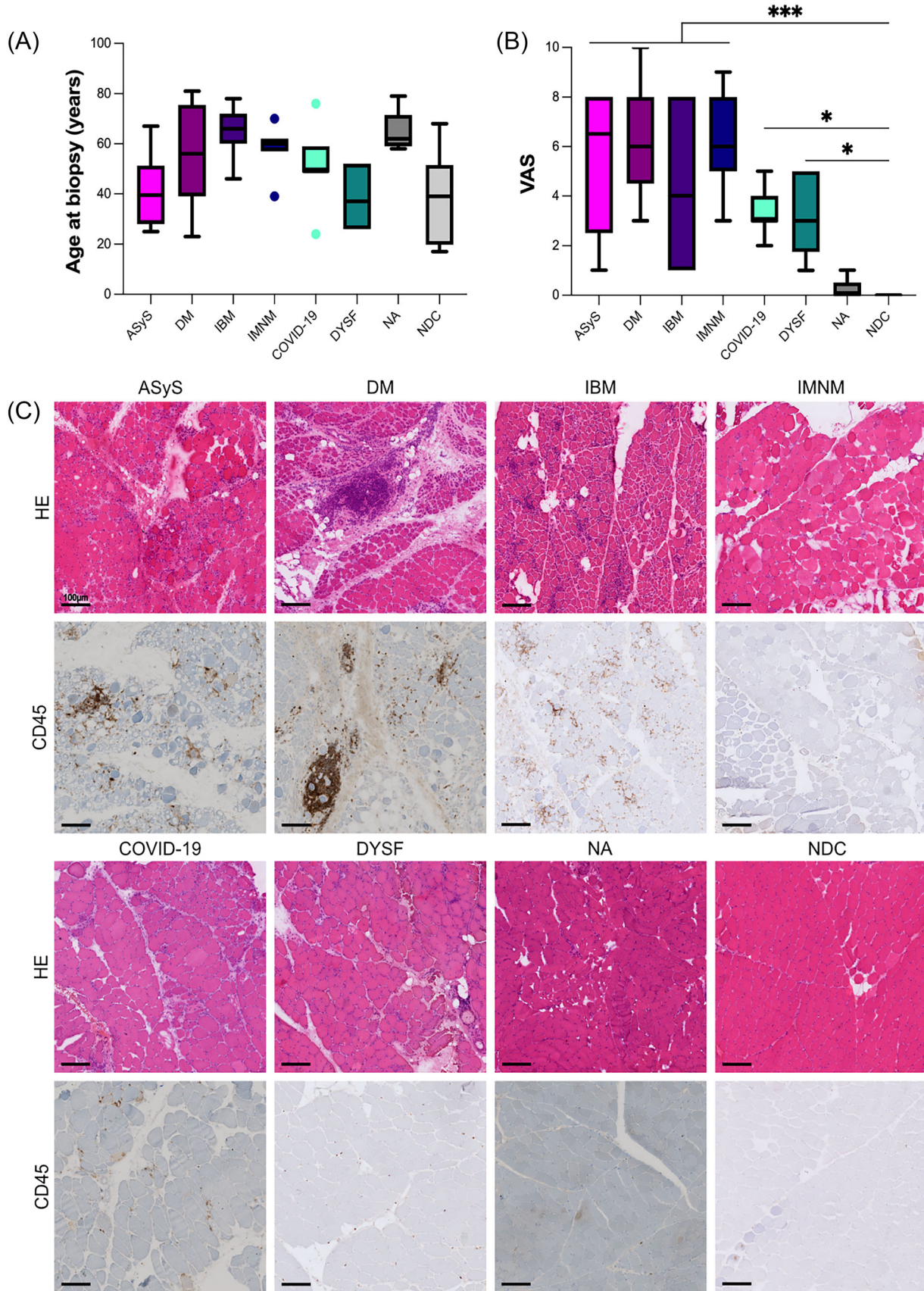
FIGURE 2 Clinical and morphological findings. Age of patients included in the study at the time of biopsy (A). Muscle pathology score (VAS) was estimated in H&E-stained sections. Groups were compared by the Kruskal–Wallis test with correction for multiple comparisons (B). Representative muscle pathology (H&E) and immune cell infiltrates (CD45) in all subgroups (C).

demographic, clinical and serological characteristics are summarised in Supplemental Table 2.

Skeletal muscle pathology reveals high pathology scores in all IIM subtypes

The detailed morphological characterisation is summarised in Supplemental Table 3. The morphological estimation of the VAS pathology score showed significantly higher scores in all IIMs than in NDC and NA, with no difference between the IIM subgroups. The VAS of the DYSF and COVID-19 cases were significantly higher than those of the NDC (Figure 2B, Supplemental Table 4). Representative H&E and CD45-stained sections are shown in Figure 2C.

Automated analysis at immunofluorescence sections provides accurate protein levels on muscle fibre and endomysial vessels

Fluorescence microscopy is a powerful tool for evaluating proteins in different cellular compartments. In this study, we analysed the co-expression of MHC-1 and MHC-2 in muscle fibres using the sarcolemmal protein spectrin. ICAM-1 expression in muscle fibre was analysed using antibodies against desmin, and expression in the endomysial vessels was analysed using the endothelial marker CD31. Supplemental Figure 1 shows representative images of an ASyS case. The merged signal (yellow) demonstrates the co-expression of MHC-1 and ICAM-1 in myofibres and vessels.

Quantification of MHC-1 and MHC-2 expression on muscle fibres shows distinct levels in myositis subgroups compared with controls

MHC-1 expression on myofibres (MOC MHC-1/spectrin) was significantly higher in ASyS, DM, IBM and COVID-19 than in NDC (Figure 3A, B). The expression of MHC-2 in myofibres (MOC MHC-2/spectrin) was significantly higher in ASyS, DM, IBM and COVID-19 than in NDC (Figure 3A, C).

Quantification of ICAM-1 expression on muscle fibres and endomysial vessels highlights endothelial activation in ASyS, DM and COVID-19

ICAM-1 shows a constitutive expression on the endothelial cells of normal muscle (NDC). ICAM-1 expression in muscle fibres (MOC ICAM-1/desmin) was significantly higher in ASyS, DM, IBM, IMNM and COVID-19 than the NDC (Figure 4A, B). ICAM-1 was expressed at a significantly higher level in the endothelial cells of ASyS, DM and COVID-19 cells than in NDC (Figure 4A, B).

The detailed statistical analyses are provided in Supplemental Table 4.

Comparison of quantified MHC-1, MHC-2 and ICAM-1 levels shows distinct protein patterns in the disease subgroups

To better visualise the quantification of MHC-1, MHC-2 and ICAM-1, we summarised their protein levels using a normalised heatmap based on the individual means of each subgroup (Supplemental Table 5). Key findings include that MHC-1 is highly expressed in muscle fibres (MOC) in ASyS, DM and IBM compared with IMNM.

The most pronounced MHC-2 expression in muscle fibres (MOC) was noted specifically in the IBM subgroup. More pronounced MHC-2 expression levels were present in ASyS than in DM. All myopathy samples exhibited higher levels of ICAM-1 in muscle fibres (MOC) than those of the NA and NDC, with the highest levels observed in IBM. Notably, a strong capillary ICAM-1 expression (MGV) was observed in ASyS, DM and COVID-19 (Figure 5A).
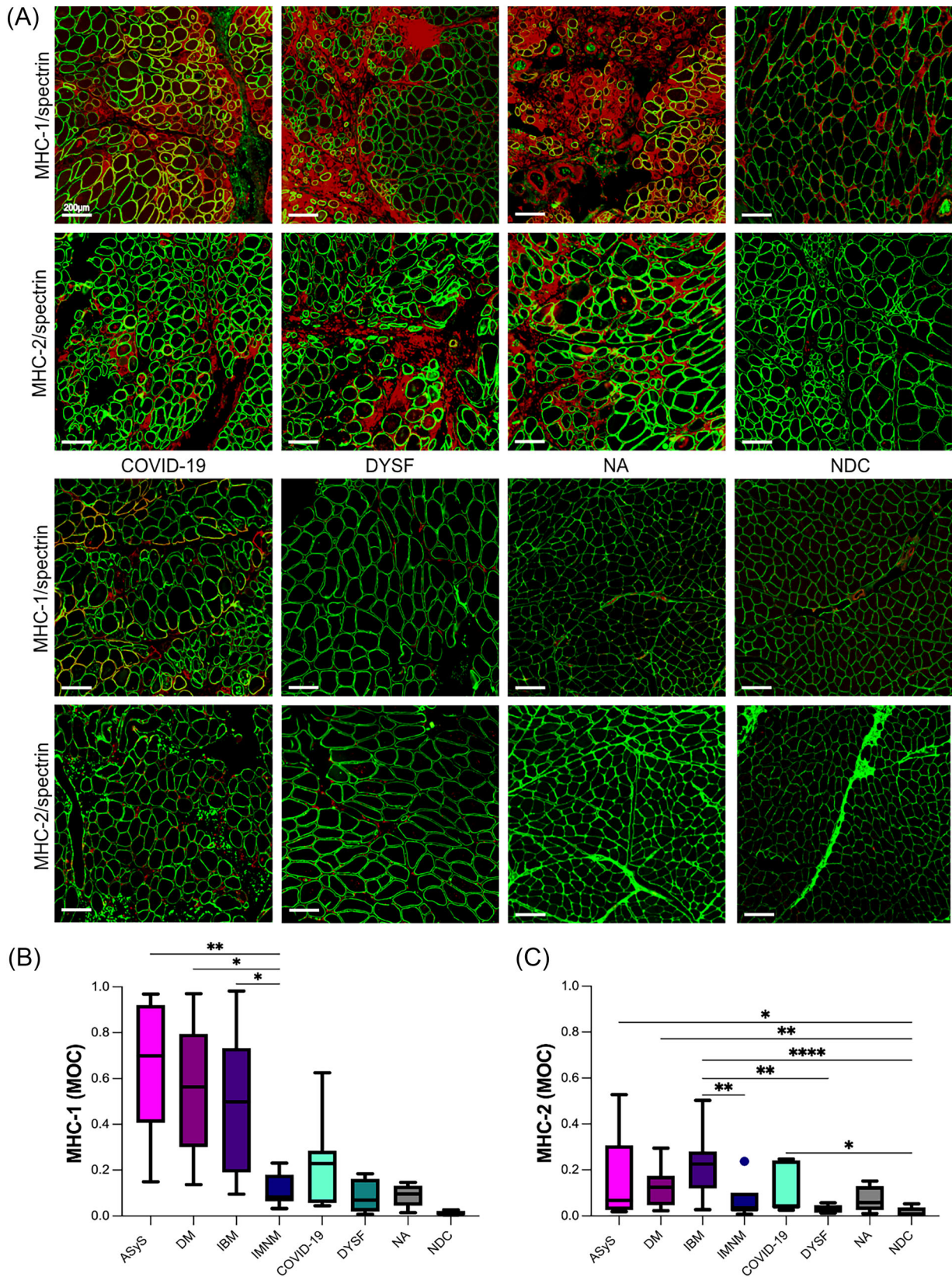
High discrimination of ICAM-1 expression in myositis subgroups

To determine ICAM-1 as a diagnostic marker for myositis, we compared the protein expression of ICAM-1 in myositis subgroups and controls by calculating ROC curves and determining the AUC [35]. The AUC discrimination was categorised as outstanding if it was ≥0.9, excellent if it was ≥0.8 and <0.9, and acceptable if it was ≥0.7 and ≤0.8 [36]. The analysis revealed that ICAM-1 expression in the endomysial vessels (MGV) significantly discriminated ASyS, DM and COVID-19 from NDC, with ASyS and COVID-19 showing higher discrimination from IBM and IMNM compared with DM. (Figure 5B). ICAM-1 on vessels demonstrated a higher specificity (>80%) in ASyS and COVID-19 than in NDC, IBM and IMNM. Similarly, ICAM-1 on muscle fibres exhibited a higher specificity (>80%) in ASyS and COVID-19 than in NDC. (Figure 5C). The detailed statistical analysis is provided in Supplemental Table 6.

Correlation of MHC-1, MHC-2 and ICAM-1 with morphological and clinical parameters demonstrates no meaningful differences between groups

Spearman's rank correlation coefficient was used to investigate the relationship between the protein expression of MHC-1, MHC-2 and ICAM-1 in ASyS, DM, IBM, IMNM and COVID-19 with morphologic parameter (VAS) and clinical parameters (CK-level). VAS was known in 100% of the biopsies. CK- levels were available for 29/40 patients (73%). Only in DM, MHC-1 showed a highly significant correlation with CK levels ($p = 0.0028$). No further statistically significant

PRECISE PROTEIN DETECTION IN MYOSITIS

Neuropathology and
Applied Neurobiology
JOURNAL OF THE BRITISH NEUROPATHOLOGICAL SOCIETY

WILEY

7 of 17

FIGURE 3 Quantification of protein expression of MHC-1 and MHC-2 on muscle fibres. Representative images of merged immunofluorescence staining show MHC-1 and MHC-2 expression in muscle fibres from different groups (A). Quantification of protein expression on muscle fibre (MOC) shows significant differences in the expression of MHC-1 (B) and MHC-2 (C) in the groups. The groups were compared by the Kruskal–Wallis test with correction for multiple comparisons.
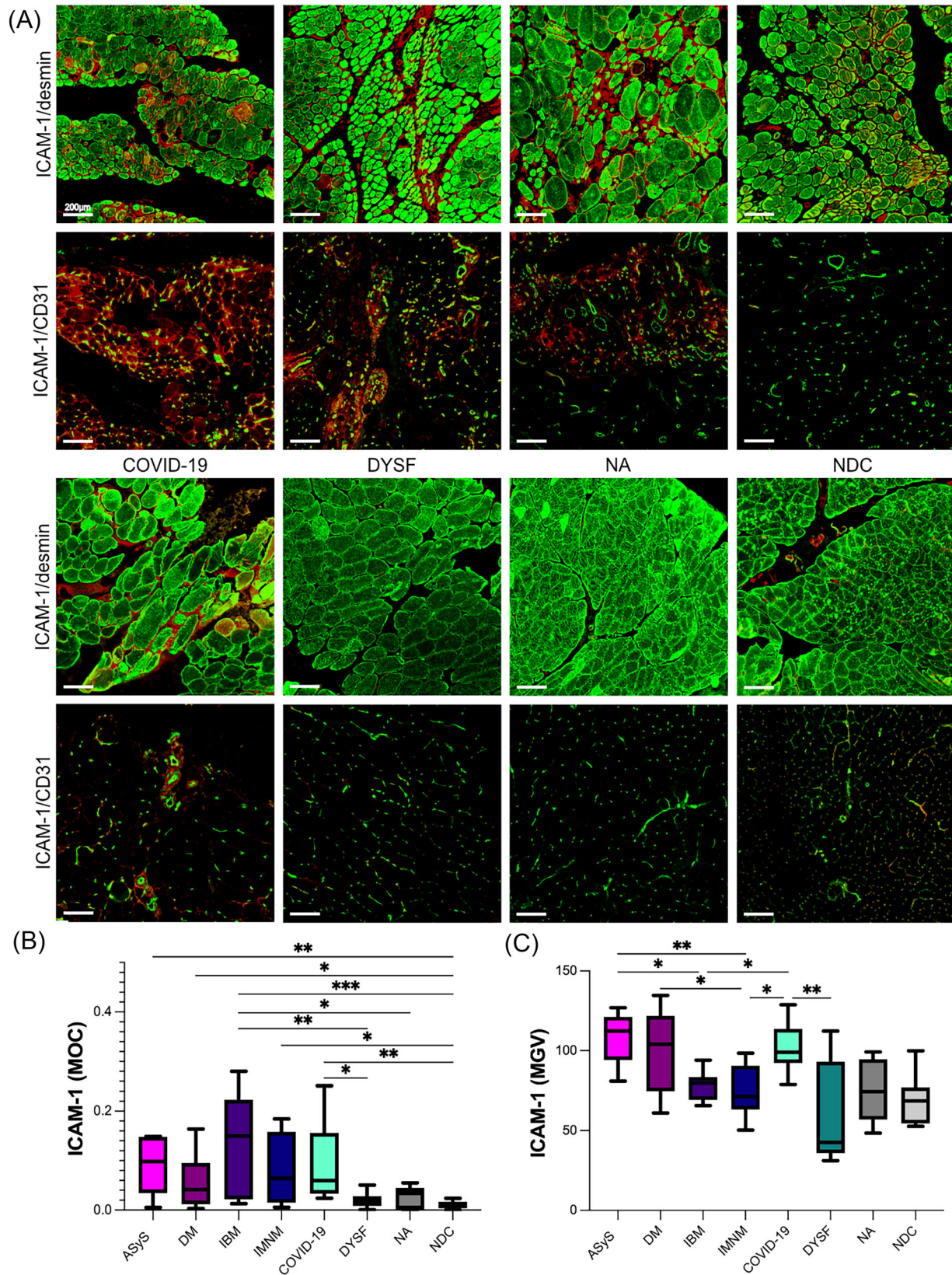
FIGURE 4 Quantification of protein expression of ICAM-1 in muscle fibres and endomysial vessels. Representative images of merged immunofluorescence staining show ICAM-1 on myofibres and endomysial capillary expression in different groups (A). Quantification of protein expression in myofibres (MOC) (B) and on endomysial vessels (MGV) (C) shows significant differences in the expression of ICAM-1 in the groups. Groups were compared by the Kruskal–Wallis test with correction for multiple comparisons.
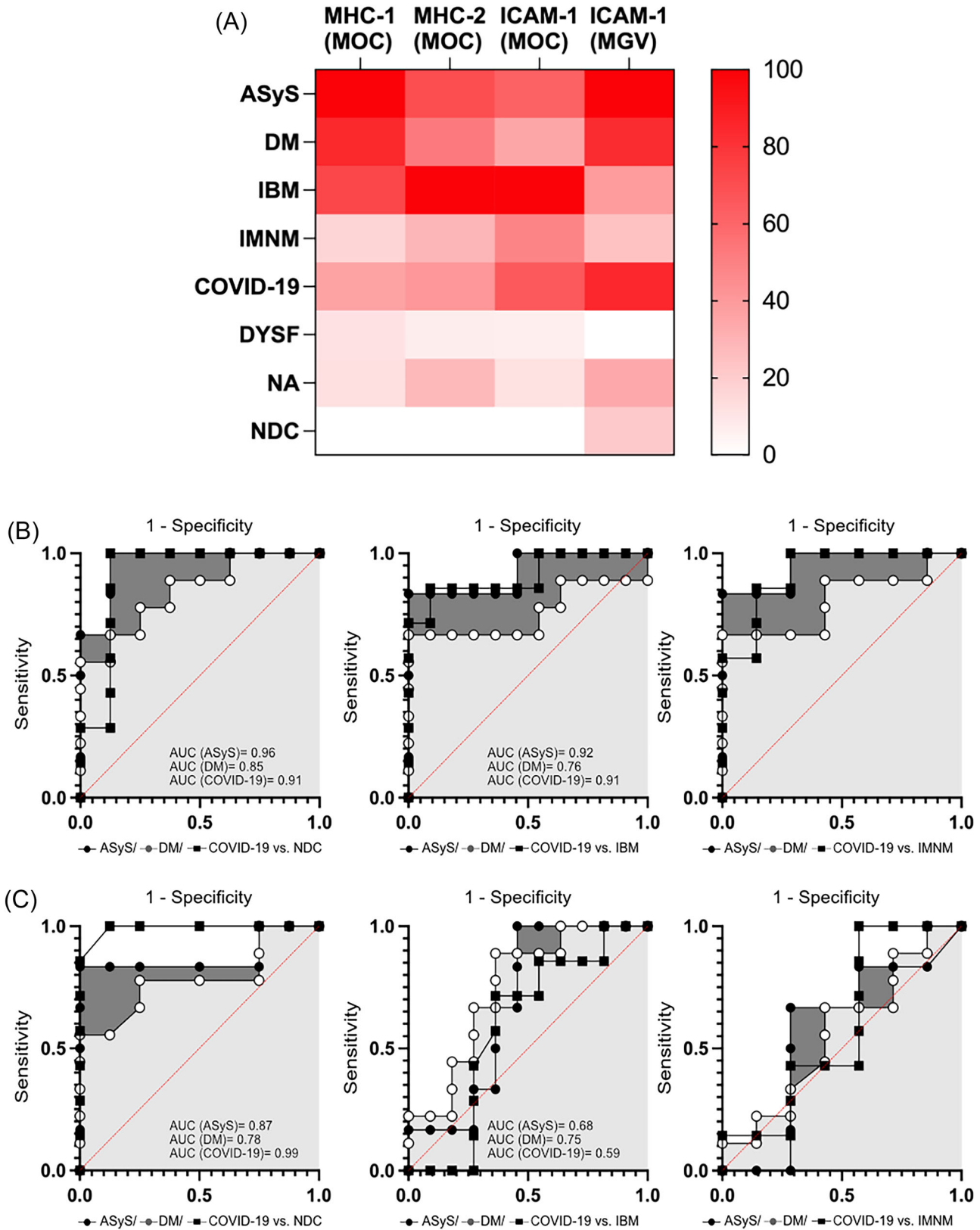
FIGURE 5 Comparison of protein expression with normalised heatmap shows different protein expression of MHC-1, MHC-2 and ICAM-1 on muscle fibres (MOC) and endomysial vessels (MGV) in the groups, revealing a diagnostic workflow for interpreting muscle pathology (A). Receiver operating characteristics analysis (ROC) of ICAM-1: ICAM-1 expression on endomysial vessels (MGV) shows significant discrimination of ASyS, DM and COVID-19 compared with NDC, IBM and IMNM (A). ICAM-1 expression on myofibres (MOV) shows significant discrimination of ASyS, DM and COVID-19 compared with NDC. (B). (AUC = area under the curve).

correlations were observed. The detailed statistical analysis is provided in Supplemental Table 4.

Bulk RNA transcriptomics confirms the expression patterns at the gene level

To corroborate these protein expression findings, we analysed muscle specimens from each group using bulk RNA transcriptomics. We included 25 patients for this approach who were also analysed in the immunofluorescence work-up and who had ASyS (n = 3), DM (n = 4), IBM (n = 3), IMNM (n = 3), COVID (n = 4), DYSF (n = 3), NA (n = 2) and NDC (n = 3) (Supplemental Table 3). At the gene level, we confirmed the expression pattern of MHC-1, MHC-2 and ICAM-1. Here, the genes encoding MHC-1 (HLA-A, HLA-B and HLA-C) were found to be elevated in ASyS, DM, IBM and COVID-19 compared with the controls (NDC), consistent with protein-level data (A). Concurrently, the genes encoding MHC-2 (HLA-DPB1, HLA-DPA1, HLA-DMB, HLA-DOA, HLA-DOB, HLA-DQA1, HLA-DQB1 and HLA-DR) were increased in ASyS, IBM, IMNM and COVID-19 compared with the controls (NDC) (B). There were slight differences in the usage of individual genes encoding either MHC-1 or MHC-2 between the disease subtypes, without a distinct pattern. At the gene level, ICAM-1 was significantly higher in ASyS, DM, IBM, IMNM and COVID-19 compared with controls (NDC) (C) (Figure 6).

Bulk RNA transcriptomics demonstrate distinct pathways in each disease subtype

To further analyse the bulk transcriptomic dataset, we performed dimensional reduction using PCA to understand the differences between the included entities. This analysis revealed that IIMs and COVID-19 segregated from the controls, whereas DYSF samples showed the highest overlap with the NDC and NA samples (Figure 7A). To provide a clearer overview, we excluded the DYSF and NA samples from the PCA (Figure 7B). The results indicated that DM, IBM and COVID-19 displayed similar transcriptomic profiles, with DM showing the greatest divergence from the control samples on the PCA. In contrast, IMNM and ASyS exhibited distinct patterns, although some overlapped with the NDC samples. To identify the specific gene pathways underlying these differences, we computed the DEGs by comparing IIM entities and COVID-19 with NDC. Each disease subtype that exhibited distinct pathways is demonstrated in Figure 7C.

Immunohistochemical DAB staining of ICAM-1 for light microscopy routine diagnostic use confirms protein patterns

Our methods for protein quantification in immunofluorescent sections require special laboratory equipment and are not useful for routine diagnostic workups. Therefore, we conducted immunohistochemistry of ICAM-1 with an automated benchmark system and DAB staining. The DAB-stained sections confirmed the ICAM-1 expression in our quantitative immunofluorescence studies. In NDC, NA and DYSF, weak staining of endomysial vessels and no staining of ICAM-1 on myofibres were observed. However, in ASyS, DM and COVID-19, a strong increase in endomysial staining was noted. An increase in myofibre staining was observed in ASyS, DM and IBM while it was less pronounced in IMNM and COVID-19 (Figure 8).

DISCUSSION

Analysis of muscle biopsies is important for the precise diagnosis of muscle diseases and for developing therapeutic strategies for individual patients. Particularly in the field of IIM, myopathological workup has significantly improved in recent years [26, 27]. In addition, analysing muscle biopsies provides important information for a deeper understanding of the underlying immune signature, thereby improving treatments. The differential diagnosis of IIM is also becoming more challenging as other conditions such as hereditary myopathies or COVID-19-associated myopathy can mimic IIM. This study aimed to characterise the protein patterns of established diagnostic markers MHC-1 and MHC-2 and, in addition, the candidate marker ICAM-1 in skeletal muscle biopsies of disease subgroups using an objective morphometric analysis tool. Specific genetic signatures were estimated by analysing bulk transcriptomics.

MHC-1 and MHC-2 have been implemented in the routine diagnostic workup of muscle pathology and reflect different interferon regulation in myositis subtypes [9–12, 14, 22, 23, 37, 38]. An overview of the studies has been recently reviewed by Nelke et al. [15]. Abnormal MHC-1 immunostaining has a high sensitivity and low specificity to distinguish IIMs from NA and other myopathies [11, 39]. In particular, MHC-2 is strongly upregulated in IBM and ASyS and is helpful in morphological diagnosis [12, 13, 40].

In previous human studies, the expression of MHC-1, MHC-2 and ICAM-1 was analysed in DAB-stained sections and assessed by subjective scoring. However, correlations with other parameters are difficult [9–11, 13, 14, 22, 23]. For this purpose, we established a tool for quantifying protein levels in different cellular compartments using immunofluorescence of whole muscle sections. The advantage of this method is that detailed analyses can be performed on limited quantities of tissue, and muscle morphology can be directly assessed in the corresponding H&E-stained sections. Using whole-section analysis, protein levels in large areas can be quantified in an observer-independent manner. The results can be correlated with other parameters or graphically visualised using a normalised heatmap. Furthermore, using imaging tools to analyse expression levels provides accurate data and is reliable for reproducibly quantifying a large number of immunofluorescent images [32]. Additionally, the unequal distribution of different skeletal muscle structures, such as endomysial capillaries, can be analysed at section level. Additionally, this method may be useful for validating molecular analysis.
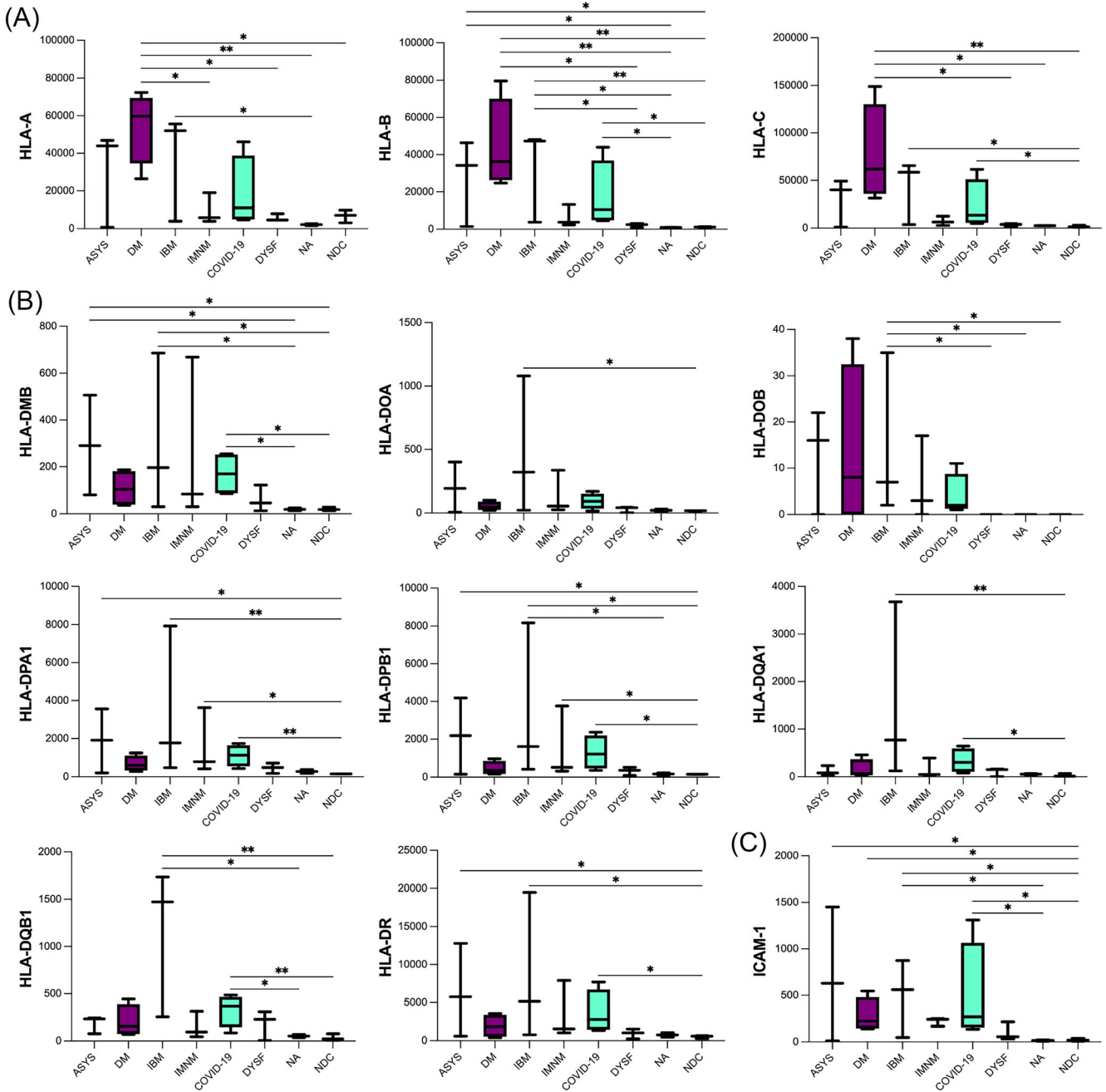
FIGURE 6 Bulk RNA transcriptomics confirms the upregulation of disease-driving proteins. Bulk RNA transcriptomics of skeletal muscle from different IIM entities. The normalised expression values are displayed on the Y-axis for each indicated gene. Expression values for genes constituting the MHC-1 comparing different IIM entities (A). Expression values for genes constituting the MHC-2 (B). Expression values for genes constituting the ICAM-1 (C). The groups were compared by the Kruskal–Wallis test with correction for multiple comparisons.

Using our method, we confirmed, that increased levels of MHC-1 could be detected on muscle fibres in IBM, DM and ASyS, and lower rates in IMNM. A comparison of the data in the normalised heatmap showed higher levels of MHC-1 and MHC-2 in IBM and ASyS than DM, consistent with previous studies introducing MHC-2 as a helpful marker for IBM and discrimination of ASyS and DM [13, 14]. However, the correlation between protein levels and muscle morphology (VAS) showed no significant differences between the groups.

Correlations with clinical parameters revealed a correlation only between MHC-1 and CK-level in the DM group.

Immune-mediated myopathies have been proposed in association with COVID-19 [7,41,42]. Skeletal muscle biopsies show non-specific myositis with varying degrees of lymphocyte infiltration and no evidence of direct viral infection [8]. Post-vaccination myositis has also been reported [43]. Therefore, identifying specific proteins that play a role in the immune processes in certain myositis subtypes may help

(A)

(B)
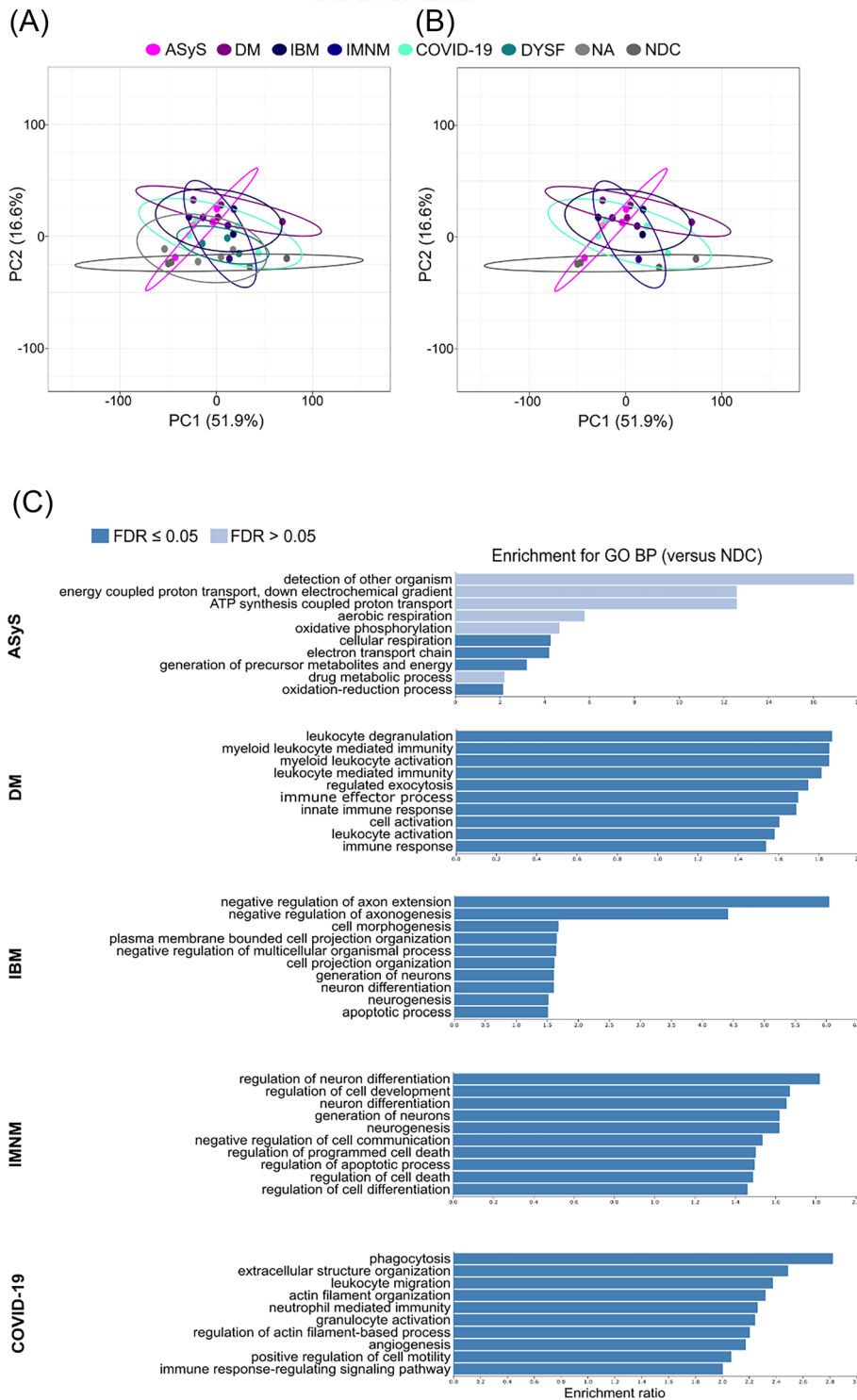
FIGURE 7 Unbiased analysis of the transcriptomics dataset. PCA showed a segregation of IIM and COVID-19 from controls and NA, while DYSF was between these groups (A). Excluding DYSF and NA from the analysis revealed that DM, IBM and COVID displayed similar transcriptomic profiles (B). The analysis of gene pathways identified significant differences in IIM entities and COVID-19 (C).

(C)

improve the diagnosis of skeletal muscle biopsies and avoid inappropriate therapies. In our study, MHC-1 and MHC-2 were significantly upregulated in SARS-CoV-2 infection-associated myopathy and post-vaccination compared with controls, highlighting an interferon-driven pathology.

ICAM-1 has been implicated in the pathophysiology of autoimmune diseases because of several immune processes, including leukocyte trafficking, leukocyte trans-endothelial migration, vascular endothelia breakdown, immune synapse formation and sustained engagement of the T-cell receptors with the MHC peptide complex [16, 44, 45]. Increased serum-soluble ICAM-1 (sICAM-1) is a marker for endothelial activation [46]. ICAM-1 is expressed by human myoblasts throughout myogenesis and is upregulated by various inflammatory stimuli, including the cytokine tumour necrosis factor-alpha (TNF), interleukin 1 beta (IL1β), interferon-gamma (IFNγ) and interleukin 6 (IL-6) [47]. ICAM-1 is a major mediator of adhesion between

FIGURE 8 ICAM-1 detection with DAB staining for routine light microscopy. Representative images of ICAM-1 expression in the DAB-stained sections demonstrate a high level of agreement with the data obtained by immunofluorescence.
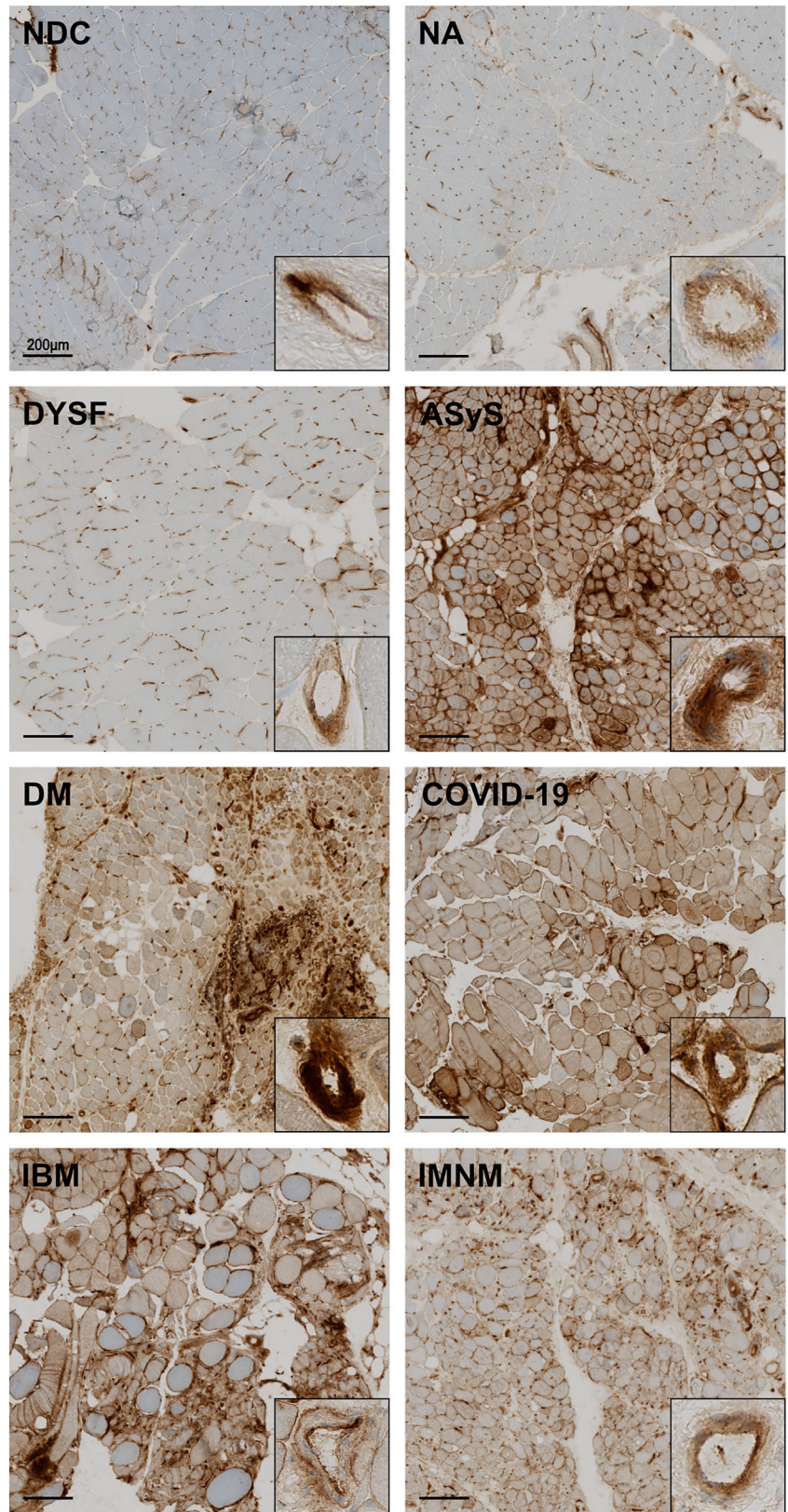
myotubes and lymphocytes through the leukocyte function-associated antigen receptor [47, 48].

In myositis, serum levels of soluble ICAM-1 are elevated [44, 49]. Initial studies by De Bleecker and Engel analysing ICAM-1 expression in muscle sections described a constitutive expression of ICAM-1 on endothelial cells in normal muscle. They also noted a selective induction of non-necrotic fibres facing invading mononuclear cells and a selective upregulation of ICAM-1 on endothelial cells in DM [21]. In

other studies, ICAM-1 expression in IBM was described on both muscle fibres and capillaries, whereas in DM, it was primarily on capillaries, showing high sensitivity but low specificity [9, 20, 23, 44, 50]. However, the role of ICAM-1 in IIM remains poorly understood. Notably, ICAM-1 expression has not been demonstrated in muscle biopsies classified in accordance with the current myositis classification.

In our analysis, ICAM-1 was strongly upregulated in the myofibres of all IIM subtypes, including IMNM, with the highest levels observed in IBM. The pronounced ICAM-1 expression in muscle fibres exhibiting partial invasion of cytotoxic lymphocytes in IBM is consistent with this function [44]. Whether the increased expression of ICAM-1 in IMNM underlies immunological pathophysiology or is due to other stimuli such as reactive oxygen species, impaired glucose metabolism or oxidative stress, should be addressed in future studies [51–54]. Several studies have demonstrated ASyS as an individual entity with distinctive interferon pathway regulation, characterised by strong IFN type 2 expression and specific morphological features [55–57]. In our study, we demonstrated a stronger upregulation of ICAM-1 in muscle fibres in ASyS than DM. More strikingly, our data indicates a strong upregulation of ICAM-1 in the endomysial capillaries in DM, ASyS and COVID-19. These findings highlight endothelial activation and multi-organ pathology, such as pulmonary and cutaneous involvement, in these entities [58, 59]. Overexpression of ICAM-1 by capillary endothelial cells in DM supports the hypothesis that vascular injury is the major pathology of this disease [21, 60]. In line with our findings, ICAM-1 expression in human lung endothelial cells can be induced by sera from patients with Jo-1-antibody-associated ASyS, highlighting the multi-organ involvement of this disease [61].

In our samples from patients with SARS-CoV-2 infection and SARS-CoV-2 vaccination-associated myositis, ICAM-1 was upregulated in muscle fibres and vessels. These findings are in line with the significantly higher serum levels of inflammatory mediators, including ICAM-1, in patients with COVID-19 [62]. Of note, we observed a strong upregulation of ICAM-1 in endomysial capillaries, which aligns with research indicating that the association between cytokine storm syndrome and endothelial damage is a significant factor in the pathology of COVID-19 [63, 64]. Notably, similar to ASyS and DM, patients with COVID-19 can present with cutaneous symptoms [59]. However, the limited number of samples included in this study is insufficient to provide a detailed explanation of the underlying pathology. Nevertheless, the results strongly suggest endothelial activation in skeletal muscles, raising questions about the significant risk factor and why certain organs are more affected than others. However, other vascular pathologies such as rarefication of endomysial capillaries, ultrastructural alterations of the vessel wall, or complement deposits were not analysed in our study [29]. Further studies are required to provide a deeper understanding of the association between ICAM-1-dependent endothelial activation and alterations in vessel morphology.

The advent of transcriptomics in the field of IIM has several advantages, including a more objective and quantitative assessment of predefined readouts independent of the investigator [65]. Here, the transcriptomic levels of MHC-1, MHC-2 and ICAM1

corresponded to the protein levels, providing data on differences between disease subtypes at two methodological levels. Currently, large-scale transcriptomic studies on bulk or single-cell/nucleus RNA levels comparing different types of IIM remain an unmet need. Nonetheless, transcriptomic assessment has already been proven to be informative in the identification of specific disease subtypes in a specific form of myositis, as recently demonstrated by Pinal-Fernandez et al., who identified distinct groups of immune checkpoint inhibitor-induced myositis [65]. A drawback of transcriptomics is that the gene level does not necessarily correlate with the protein level and, by extension, with functional consequences. Consequently, transcriptomic studies should be accompanied by immunohistopathological assessments to provide a robust and comprehensive analysis.

Using PCA, the IIM spectrum and COVID-19 were segregated from the controls and NA, whereas the DYSF group was intermediate between the former two. Given the unbiased approach of bulk transcriptomics, this observation points to inflammation as a shared pathway between IIM and COVID-19, underlying the distinction in PCA analysis. Among the inflammatory muscle diseases, DM, IBM and COVID-19 displayed shared clustering whereas IMNM and ASyS were distinct. Previous transcriptomic data suggested that ASyS, IBM and DM share a strong interferon type 2 signature, while DM and ASyS are characterised by interferon type 1 [56]. We speculate that, at the level of bulk transcriptomics, a shared signal of interferon and inflammatory pathways might underlie the observed pattern of clusters. In a previous study, Amici et al. demonstrated that transcriptomic profiles displayed sufficient differences between IIM entities to enable an unbiased differentiation of specific IIM subtypes [66]. Further analysis revealed distinct gene pathways for each IIM subtype and COVID-19. Notably, in our dataset, the ASyS samples were enriched for genes related to energy metabolism, whereas the DM samples were characterised by a strong signature of immune-related pathways. We suspect that these observations align with previous transcriptomic analyses showing pronounced interferon type 1 in DM, whereas ASyS is characterised by a loss of muscle function and redox reactions, potentially pointing to impaired energy metabolism [66]. Furthermore, IBM was enriched in pathways related to the negative regulation of axon extension, possibly connected to recent reports from our laboratory suggesting a specific loss of NMJs in the IIM subtype [67]. The observation of the regulation of cell death/development in IMNM could indicate necrosis and regeneration of muscle cells in this disease [68]. Notably, we also provided data on COVID-19 at the transcriptomic level, revealing enrichment of pathways such as leukocyte migration, cell motility and immune response, which are a group of gene pathways related to ICAM-1. These data align with the increased protein levels of ICAM-1 observed at the immunohistochemical level. Taken together, IIM subtypes were characterised by distinct gene pathways warranting further research into their distinct functional consequences.

In conclusion, we have provided quantitative data on immune-associated proteins, such as MHC-1, MHC-2 and ICAM-1, at the protein and gene levels and identified specific gene pathways that can be integrated into our pathophysiological understanding of IIM. Our data

confirm previous findings on MHC-1 and MHC-2 expression and highlight the role of MHC-2 in myositis pathology with upregulation in IBM and ASyS. Notably, ICAM-1 expression provides distinct immune signatures in various myositis subgroups and in patients with SARS-CoV-2-associated myopathy. There is evidence that the vascular pathology observed in ASyS, DM and COVID-19 may be associated with ICAM-1-mediated endothelial activation. Furthermore, our data introduced ICAM-1 as a new specific diagnostic marker for the morphological classification of myositis. In future studies, the specificity of ICAM-1 expression in DAB stained sections should be analysed in a larger cohort of IIM subtypes, including different serological entities.

ETHICS APPROVAL AND CONSENT TO PARTICIPATE

This project was approved by the local ethics committee (AZ 07/09 Justus Liebig University Giessen, Germany) and conducted in accordance with the Declaration of Helsinki.

AVAILABILITY OF DATA AND MATERIALS

The transcriptomic data has been deposited under Gene Expression Omnibus (GEO) GSE260786.

AUTHORS' CONTRIBUTION

Conceptualization: AS, TR Methodology: AS, AN, CN, TR, AR. Formal analysis and investigation: AS, AN, CN. Writing - original draft preparation: AS, AN, CN. Writing - review and editing: WS, MH, AM, CO, BZ, HHK, EBJ, UML. Funding acquisition: AS, TR. Resources: AS, TR; Supervision: AS, TR All authors have read and approved the final manuscript.

CONFLICT OF INTEREST STATEMENT
The Editors of Neuropathology and Applied Neurobiology are committed to peer-review integrity and upholding the highest standards of review. As such, this article was peer-reviewed by independent, anonymous expert referees and the authors (WS) had no role in either the editorial decision or the handling of the paper.

DATA AVAILABILITY STATEMENT
The data that supports the findings of this study are available in the supplementary material of this article

ORCID
Alexander Mensch https://orcid.org/0000-0003-0089-4473
Werner Stenzel https://orcid.org/0000-0002-1143-2103
Anne Schänzer https://orcid.org/0000-0002-2014-2028

REFERENCES

1. Allenbach Y, Benveniste O, Goebel HH, Stenzel W. Integrated classification of inflammatory myopathies. Neuropathol Appl Neurobiol. 2017; 43: 62–81. 10.1111/nan.12380.
2. Tanboon J, Uruha A, Stenzel W, Nishino I. Where are we moving in the classification of idiopathic inflammatory myopathies? Curr Opin Neurol. 2020; 33: 590–603. 10.1097/wco.0000000000000855.
3. Lundberg IE, Fujimoto M, Vencovsky J, Aggarwal R, Holmqvist M, Christopher-Stine L, Mammen AL, Miller FW. Idiopathic inflammatory myopathies. Nat Rev Dis Primers. 2021; 7: 86. 10.1038/s41572-021-00321-x.
4. Benveniste O, Romero NB. Myositis or dystrophy? Traps and pitfalls. *Presse Med.* 2011;40(4):e249–e255. 10.1016/j.lpm.2010.11.023
5. Becker N, Moore SA, Jones KA. The inflammatory pathology of dysferlinopathy is distinct from calpainopathy, Becker muscular dystrophy, and inflammatory myopathies. Acta Neuropathol Commun. 2022; 10: 17. doi 10.1186/s40478-022-01320-z.
6. Choi J-H, Park Y-E, Kim S-I, Kim J-I, Lee C-H, Park K-H, Kim D-S. Differential immunohistological features of inflammatory myopathies and dysferlinopathy. J Korean Med Sci. 2009; 24: 1015–1023. 10.3346/jkms.2009.24.6.1015.
7. Aschman T, Schneider J, Greuel S, Meinhardt J, Streit S, Goebel HH, Büttnerova I, Elezkurtaj S, Scheibe F, Radke J, Meisel C, Drosten C, Radbruch H, Heppner FL, Corman VM, Stenzel W. Association Between SARS-CoV-2 Infection and Immune-Mediated Myopathy in Patients Who Have Died. JAMA Neurol. 2021; 78(8): 948–960. 10.1001/jamaneurol.2021.2004.
8. Aschman T, Stenzel W. COVID-19 associated myopathy. Curr Opin Neurol. 2022; 35: 622–628. 10.1097/wco.0000000000001101.
9. Bartoccioni E, Gallucci S, Scuderi F, Ricci E, Servidei S, Broccolini A, Tonali P. MHC class I, MHC class II and intercellular adhesion molecule-1 (ICAM-1) expression in inflammatory myopathies. Clin Exp. Immunol. 1994;95: 166–172. doi 10.1111/j.1365-2249.1994.tb06032.x.
10. Rodríguez Cruz PM, Luo YB, Miller J, Junckerstorff RC, Mastaglia FL, Fabian V. An analysis of the sensitivity and specificity of MHC-I and MHC-II immunohistochemical staining in muscle biopsies for the diagnosis of inflammatory myopathies. Neuromuscul Disord. 2014; 24: 1025–1035. doi 10.1016/j.nmd.2014.06.436.
11. Milisenda JC, Pinal-Fernandez I, Lloyd TE, Grau-Junyent JM, Christopher-Stine L, Corse AM, Mammen AL. The pattern of MHC class I expression in muscle biopsies from patients with myositis and other neuromuscular disorders. Rheumatology (Oxford). 2023; 62: 3156–3160. doi 10.1093/rheumatology/kead052.
12. Emslie-Smith AM, Arahata K, Engel AG. Major histocompatibility complex class I antigen expression, immunolocalization of interferon subtypes, and T cell-mediated cytotoxicity in myopathies. Hum Pathol. 1989; 20: 224–231. doi:10.1016/0046-8177(89)90128-7.
13. Aouizerate J, De Antonio M, Bassez G, Gherardi RK, Berenbaum F, Guillevin L, Berezne A, Valeyre D, Maisonobe T, Dubourg O, Cosnes A, Benveniste O, Authier FJ. Myofiber HLA-DR expression is a distinctive biomarker for antisynthetase-associated myopathy. Acta Neuropatholog Commun. 2014; 23: 2:154. doi 10.1186/s40478-014-0154-2.
14. Tanboon J, Inoue M, Hirakawa S, Tachimori H, Hayashi S, Noguchi S, Okiyama N, Fujimoto M, Suzuki S, Nishino I. Muscle pathology of antisynthetase syndrome according to antibody subtypes. Brain Pathol. 2023; 33: e13155. doi:10.1111/bpa.13155.
15. Nelke C, Schmid S, Kleefeld F, et al. Complement and MHC patterns can provide the diagnostic framework for inflammatory neuromuscular diseases. *Acta Neuropathol.* 2024;147(1):15. doi:10.1007/s00401-023-02669-8
16. Haydinger CD, Ashander LM, Tan ACR, Smith JR. Intercellular adhesion molecule 1: more than a leukocyte adhesion molecule. Biology. 2023; 12: 743. 10.3390/biology12050743, 5.

17. Zonneveld R, Martinelli R, Shapiro NI, Kuijpers TW, Plötz FB, Carman CV. Soluble adhesion molecules as markers for sepsis and the potential pathophysiological discrepancy in neonates, children and adults. *Criti Care*. 2014;18:1-14. doi:10.1186/cc1373

18. Muntjewerff EM, Meesters LD, Bogaart G, Revelo NH. Reverse signaling by MHC-I molecules in immune and non-immune cell types. *Front Immunol*. 2020;11:605958. doi:10.3389/fimmu.2020.605958.19

19. Bhattarai S, Ghannam K, Krause S, Benveniste O, Marg A, de Bruin G, Xin B-T, Overkleeft HS, Spuler S, Stenzel W., Feist E. The immunoproteasomes are key to regulate myokines and MHC class I expression in idiopathic inflammatory myopathies. J Autoimmun. 2016; 75: 118–129. 10.1016/j.jaut.2016.08.004.

20. Vianna MA, Borges CT, Borba EF, Caleiro MT, Bonfá E, Marie SK. Myositis in mixed connective tissue disease: a unique syndrome characterized by immunohistopathologic elements of both polymyositis and dermatomyositis. Arq Neuropsiquiatr. 2004; 62: 923–934. 10.1590/s0004-282x2004000600001.

21. De Bleecker JL, Engel AG. Expression of cell adhesion molecules in inflammatory myopathies and Duchenne dystrophy. *J Neuropathol Exp Neurol*. 1994;53(4):369-376. doi:10.1097/00005072-199407000-00008

22. Sallum AM, Kiss MH, Silva CA, Wakamatsu A, Vianna MA, Sachetti S, Marie SK. Difference in adhesion molecule expression (ICAM-1 and VCAM-1) in juvenile and adult dermatomyositis, polymyositis and inclusion body myositis. Autoimmun Rev. 2006; 5: 93–100. 10.1016/j.autrev.2005.05.008.

23. Jain A, Sharma M, Sarkar C, Singh S, Handa R. Increased expression of cell adhesion molecules in inflammatory myopathies: diagnostic utility and pathogenetic insights. Folia Neuropathol. 2009; 47: 33–42

24. Mammen AL, Allenbach Y, Stenzel W, Benveniste O. 239th ENMC international workshop: classification of dermatomyositis, Amsterdam, the Netherlands, 14-16 December 2018. *Neuromuscul Disord*. 2020;30(1):70-92. doi:10.1016/j.nmd.2019.10.005

25. Dubowitz V, Sewry CA, Oldfords A. *Muscle biopsy: a practical approach*. 5th ed. Elsevier Limited; 2021. 5th edition.

26. De Bleecker JL, Lundberg IE, de Visser M. 193rd ENMC international workshop pathology diagnosis of idiopathic inflammatory myopathies 30 November - 2 December 2012, Naarden. *The Netherlands. Neuromusc Disord*. 2013;23(11):945-951. doi:10.1016/j.nmd.2013.07.007

27. De Bleecker JL, De Paepe B, Aronica E, de Visser M, Amato A, Benveniste O, De Bleecker J, de Boer O, Dimachkie M, Gherardi R, Goebel HH, Hilton-Jones D, Holton J, Lundberg IE, Mammen A, Mastaglia F, Nishino I, Rushing E, Schroder HD, Selcen D, Stenzel W. 205th ENMC International Workshop: Pathology diagnosis of idiopathic inflammatory myopathies part II 28–30 March 2014, Naarden, The Netherlands. Neuromusc Disord. 2015; 25 (3):268-72. doi: 10.1016/j.nmd.2014.12.001.

28. Wedderburn LR, Varsani H, Li CK, Newton KR, Amato AA, Banwell B, Bove KE, Corse AM, Emslie-Smith A, Harding B, Hoogendijk J, Lundberg IE, Marie S, Minetti C, Nennesmo I, Rushing EJ, Sewry C, Charman SC, Pilkington CA, Holton JL. International consensus on a proposed score system for muscle biopsy evaluation in patients with juvenile dermatomyositis: a tool for potential use in clinical trials. Arthritis Rheum.2007; 57: 1192–1201. doi:10.1002/art.23012.

29. Schänzer A, Rager L, Dahlhaus I, Dittmayer C, Preusse C, Della Marina A, Goebel H-H, Hahn A, Stenzel W. Morphological Characteristics of Idiopathic Inflammatory Myopathies in Juvenile Patients. Cells. 2021; 11: 109. doi:10.3390/cells11010109.

30. Aaron JS, Taylor AB, Chew TL. Image co-localization - co-occurrence versus correlation. J Cell Sci. 2018; 8;131(3):jcs211847. doi:10.1242/jcs.211847

31. Dunn KW, Kamocka MM, McDonald JH. A practical guide to evaluating colocalization in biological microscopy. Am J Physiol Cell Physiol. 2011; 300 C723-C742. doi:10.1152/ajpcell.00462.2010.

32. Shihan MH, Novo SG, Le Marchand SJ, Wang Y, Duncan MK. A simple method for quantitating confocal fluorescent images. Biochem Biophys Rep. 2021; 25: 100916. doi:10.1016/j.bbrep.2021.100916.

33. Schisterman EF, Faraggi D, Reiser B, Hu J. Youden index and the optimal threshold for markers with mass at zero. *Stad Med*. 2008; 27(2):297-315. doi:10.1002/sim.2993

34. Thomas PD. The gene ontology and the meaning of biological function. *Methods Mol Biol.*. 2017;1446:15-24. doi:10.1007/978-1-4939-3743-1_2

35. Hajian-Tilaki K. Receiver operating characteristic (ROC) curve analysis for medical diagnostic test evaluation. *Caspian J Intern Med*. 2013; 4(2):627-635. doi:10.1002/sim.2993

36. Hosmer DW, Lemeshow S, Sturdivant R. *Applied logistic regression*. 2nd ed. Wiley; 2000. doi:10.1002/0471722146

37. Bolko L, Jiang W, Tawara N, Landon-Cardinal O, Anquetil C, Benveniste O, Allenbach Y. The role of interferons type I, II and III in myositis: A review. Brain Pathol. 2021; 31: e12955. doi 10.1111/bpa.12955.

38. Tews DS, Goebel HH. Cytokine expression profile in idiopathic inflammatory myopathies. J Neuropathol Exp Neurol.1996; 55: 342–347. doi:10.1097/00005072-199603000-00009.

39. Kurdi M, Alshareef A, Bamaga AK, Fadel ZT, Alrawaili MS, Hakamy S, Mohamed F, Abuzinadah AR, Addas BM, Butt NS. The assessment of major histocompatibility complex (MHC) class-I expression in different neuromuscular diseases. Degener Neurol Neuromuscul Dis. 2021; 61–68. doi:10.2147/DNND.S340117.

40. Tanboon J, Inoue M, Hirakawa S, et al. Muscle pathology of anti-synthetase syndrome according to antibody subtypes. *Brain Pathol* 2023;33(4):e13155. doi:10.1111/bpa.13155

41. Guidon AC, Amato AA. COVID-19 and neuromuscular disorders. Neurology. 2020; 94: 959–969. 10.1212/wnl.0000000000009566.

42. Pitscheider L, Karolyi M, Burkert FR, Helbok R, Wanschitz JV, Horlings C, Pawelka E, Omid S, Traugott M, Seitz T, Zoufaly A, Lindeck-Pozza E, Wöll E, Beer R, Seiwald S, Bellmann-Weiler R, Hegen H, Löscher WN. Muscle involvement in SARS-CoV-2 infection. Eur J Neurol. 2021; 28:3411-3417. doi: 10.1111/ene.14564.

43. Syrmou V, Liaskos C, Ntavari N, et al. COVID-19 vaccine-associated myositis: a comprehensive review of the literature driven by a case report. *Immunol Res*. 2023;71(4):537-546. doi:10.1007/s12026-023-09368-2

44. Figarella-Branger D, Civatte M, Bartoli C, Pellissier JF. Cytokines, chemokines, and cell adhesion molecules in inflammatory myopathies. Muscle Nerve. 2003; 28: 659–682. doi:10.1002/mus.10462.

45. Grakoui A, Bromley SK, Sumen C, et al. The immunological synapse: a molecular machine controlling T cell activation. *Science*. 1999; 285(5425):221-227. doi:10.1126/science.285.5425.221

46. Videm V, Albrigtsen M. Soluble ICAM-1 and VCAM-1 as markers of endothelial activation. Scand J Immunol. 2008; 67: 523–531. doi:10.1111/j.1365-3083.2008.02029.x.

47. Beauchamp J, Abraham D, Bou-Gharios G, Partridge T, Olsen I. Expression and function of heterotypic adhesion molecules during differentiation of human skeletal muscle in culture. *Am J Pathol*. 1992;140:387.

48. Afzali AM, Müntefering T, Wiendl H, Meuth SG, Ruck T. Skeletal muscle cells actively shape (auto) immune responses. *Autoimmun Rev*. 2018;17(5):518-529. doi:10.1016/j.autrev.2017.12.005

49. Kumamoto T, Abe T, Ueyama H, Sugihara R, Shigenaga T, Tsuda T. Elevated soluble intercellular adhesion molecules-1 in inflammatory myopathy. *Acta Neurol Scand*. 1997; 95;34-37. doi:10.1111/j.1600-0404.1997.tb00065.x

50. Grundtman C, Salomonsson S, Dorph C, Bruton J, Andersson U, Lundberg IE. Immunolocalization of interleukin-1 receptors in the

sarcolemma and nuclei of skeletal muscle in patients with idiopathic inflammatory myopathies. *Arthritis Rheum*. 2007;56(2):674-687. doi:10.1002/art.22388

51. Roebuck KA, Rahman A, Lakshminarayanan V, Janakidevi K, Malik AB. H2O2 and tumor necrosis factor-α activate intercellular adhesion molecule 1 (ICAM-1) gene transcription through distinct cis-regulatory elements within the ICAM-1 promoter. J Biol Chem. 1995; 270: 18966–18974. doi:10.1074/jbc.270.32.18966.

52. Roebuck KA, Finnegan A. Regulation of intercellular adhesion molecule-1 (CD54) gene expression. J Leukos Biol. 1999; 66: 876–888. doi:10.1002/jlb.66.6.876.

53. Morigi M, Zoja C, Figliuzzi M, et al. Fluid shear stress modulates surface expression of adhesion molecules by endothelial cells. *Blood*. 1995;85(7):1696-1703. doi:10.1182/blood.V85.7.1696.bloodjournal8571696

54. Morigi M, Angioletti S, Imberti B, Donadelli R, Micheletti G, Figliuzzi M, Remuzzi A, Zoja C, Remuzzi G. Leukocyte-endothelial interaction is augmented by high glucose concentrations and hyperglycemia in a NF-kB-dependent fashion. J Clin Invest. 1998; 101: 1905-1915. doi:10.1172/JCI656.

55. Mescam-Mancini L, Allenbach Y, Hervier B, Devilliers H, Mariampillay K, Dubourg O, Maisonobe T, Gherardi R, Mezin P, Preusse C, Stenzel W, Benveniste O. Anti-Jo-1 antibody-positive patients show a characteristic necrotizing perifascicular myositis. Brain. 2015; 138: 2485–2492. doi 10.1093/brain/awv192.

56. Pinal-Fernandez I, Casal-Dominguez M, Derfoul A, Pak K, Plotz P, Miller FW, Milisenda JC, Grau-Junyent JM, Selva-O'Callaghan A, Paik J, Albayda J, Christopher-Stine L, Lloyd TE, Corse AM, Mammen AL. Identification of distinctive interferon gene signatures in different types of myositis. Neurology. 2019; 93: e1193-e1204. doi 10.1212/wnl.0000000000008128.

57. Uruha A, Suzuki S, Suzuki N, Nishino I. Perifascicular necrosis in anti-synthetase syndrome beyond anti-Jo-1. *Brain*. 2016;139(9):139. doi:10.1093/brain/aww125

58. Grundtman C, Lundberg IE. Vascular involvement in the pathogenesis of idiopathic inflammatory myopathies. Autoimmunity. 2009: 42: 615–626. doi:10.1080/08916930903002511.

59. Martora F, Villani A, Fabbrocini G, Battista T. COVID-19 and cutaneous manifestations: a review of the published literature. *J Cosm Dermatol*. 2023;22(1):4-10. doi:10.1111/jocd.15477

60. Cid M-C, Grau J-M, Casademont J, Tobias E, Picazo A, Coll-Vinent B, Esparza J, Pedrol E, Urbano-Márquez A. Leucocyte/endothelial cell adhesion receptors in muscle biopsies from patients with idiopathic inflammatory myopathies (IIM). Clin Exp Immunol. 1996; 104: 467–73.

61. Helmers SB, Englund P, Engström M, Åhlin E, Fathi M, Janciauskiene S, Heimbürger M, Rönnelid J, Lundberg IE. Sera from anti–Jo-1–positive patients with polymyositis and interstitial lung disease induce expression of intercellular adhesion molecule 1 in human lung endothelial cells. Arthritis Rheum. 2009; 60: 2524–2530. doi:10.1002/art.24683.

62. Tufa A, Gebremariam TH, Manyazewal T, Getinet T, Webb D-L, Hellström PM, Genet S. Inflammatory mediators profile in patients hospitalized with COVID-19: A comparative study. Front Immunol. 2022; 13: 964179. doi:10.3389/fimmu.2022.964179.

63. Karki R, Sharma BR, Tuladhar S, Williams EP, Zalduondo L, Samir P, Zheng M, Sundaram B, Banoth B, Malireddi RS. Synergism of TNF-α and IFN-γ triggers inflammatory cell death, tissue damage, and mortality in SARS-CoV-2 infection and cytokine shock syndromes. Cell. 2021; 184: 149–168. doi:10.1016/j.cell.2020.11.025.

64. Gupta A, Madhavan MV, Sehgal K, et al. Extrapulmonary manifestations of COVID-19. *Nat Med*. 2020;26(7):1017-1032. doi:10.1038/s41591-020-0968-3

65. Pinal-Fernandez I, Quintana A, Milisenda JC, et al. Transcriptomic profiling reveals distinct subsets of immune checkpoint inhibitor induced myositis. *Ann Rheum Dis*. 2023;82(6):829-835. doi:10.1136/ard-2022-223792.

66. Amici DR, Pinal-Fernandez I, Christopher-Stine L, Mammen AL, Mendillo ML. A network of core and subtype-specific gene expression programs in myositis. *Acta Neuropathol*. 2021;142(5):887-898. doi:10.1007/s00401-021-02365-5

67. Nelke C, Schroeter CB, Theissen L, et al. Senescent fibro-adipogenic progenitors are potential drivers of pathology in inclusion body myositis. *Acta Neuropathol*. 2023;146(5):725-745. doi:10.1007/s00401-023-02637-2

68. Allenbach Y, Benveniste O, Stenzel W, Boyer O. Immune-mediated necrotizing myopathy: clinical features and pathogenesis. *Nat Rev Rheumatol*. 2020;16(12):689-701. doi:10.1038/s41584-020-00515-9

SUPPORTING INFORMATION

Additional supporting information can be found online in the Supporting Information section at the end of this article.

How to cite this article: Nishimura A, Nelke C, Huber M, et al. Differentiating idiopathic inflammatory myopathies by automated morphometric analysis of MHC-1, MHC-2 and ICAM-1 in muscle tissue. *Neuropathol Appl Neurobiol*. 2024;50 (4):e12998. doi:10.1111/nan.12998